From mountains to cities: a novel isotope hydrological assessment of a tropical water distribution system

Preprint · July 2020

8 authors, including:


Ricardo Sánchez-Murillo
National University of Costa Rica
155 PUBLICATIONS **497** CITATIONS
SEE PROFILE


Germain Esquivel Hernández
National University of Costa Rica
102 PUBLICATIONS **285** CITATIONS
SEE PROFILE


Christian Birkel
University of Costa Rica
157 PUBLICATIONS **2,070** CITATIONS
SEE PROFILE


Lucia Ortega
International Atomic Energy Agency (IAEA)
17 PUBLICATIONS **39** CITATIONS
SEE PROFILE

From mountains to cities: a novel isotope hydrological assessment of a tropical water distribution system

Sánchez-Murillo R[a*], Esquivel-Hernández, G[a], Birkel, C[b], Ortega, L[d], Sánchez-Guerrero, M[e], Rojas-Jiménez, L. D[e], Vargas-Víquez, J[e]., Castro-Chacón, L[e].

[a]Stable Isotopes Research Group and Water Resources Management Laboratory, School of Chemistry, Universidad Nacional, Costa Rica, 86-3000
[b]Department of Geography and Water and Global Change Observatory, University of Costa Rica, San José, Costa Rica
[c]International Atomic Energy Agency, Isotope Hydrology Section, Vienna International Center, Vienna, Austria; [e]Empresa de Servicios Públicos de Heredia (ESPH), Costa Rica, 26-3000

*Corresponding Author (ricardo.sanchez.murillo@una.cr)

Abstract

Water use by anthropogenic activities in the face of climate change is posing a need to better understand connections between headwater sources and lowland urban water allocations. In Costa Rica over 700 water conflicts emerged over the last decade in response to limited water availability caused by prolonged droughts and inefficient water use and distribution. Here, we constrained a Bayesian mixing model with water stable isotope data (2018-2019) in rainfall (N=704), spring water (N=96), and surface water (N=94) with seasonal isotope sampling (wet and dry seasons) of an urban aqueduct (N=215) in the Central Valley of Costa Rica. Overall, low $\delta^{18}O$ rainfall compositions corresponded to the western boundary of the study area, whereas high values were reported to the northeastern limit, reflecting the influence of moisture transport from the Caribbean domain coupled with strong orographic effects over the Pacific slope. The latter is well-depicted in the relative rainfall contributions (west versus east) in two headwater systems: a) spring (68.7 ± 3.4 %, west domain) and b) stream (55.8 ± 3.9 %, east domain). The Bayesian mixing model indicated that the aqueduct exhibited a spatial predominance of spring water and surface water during a normal wet season (78.7 %), whereas deep groundwater and spring water appeared to be fundamental water sources for the aqueduct in the dry season (69.4 %). Our stable isotope approach can help improve aqueduct management practices in a changing climate including optimal source water allocation or reducing evaporative losses in the dry season.

Keywords: Costa Rica; urban hydrology; stable isotopes; Bayesian mixing model; aqueduct management.

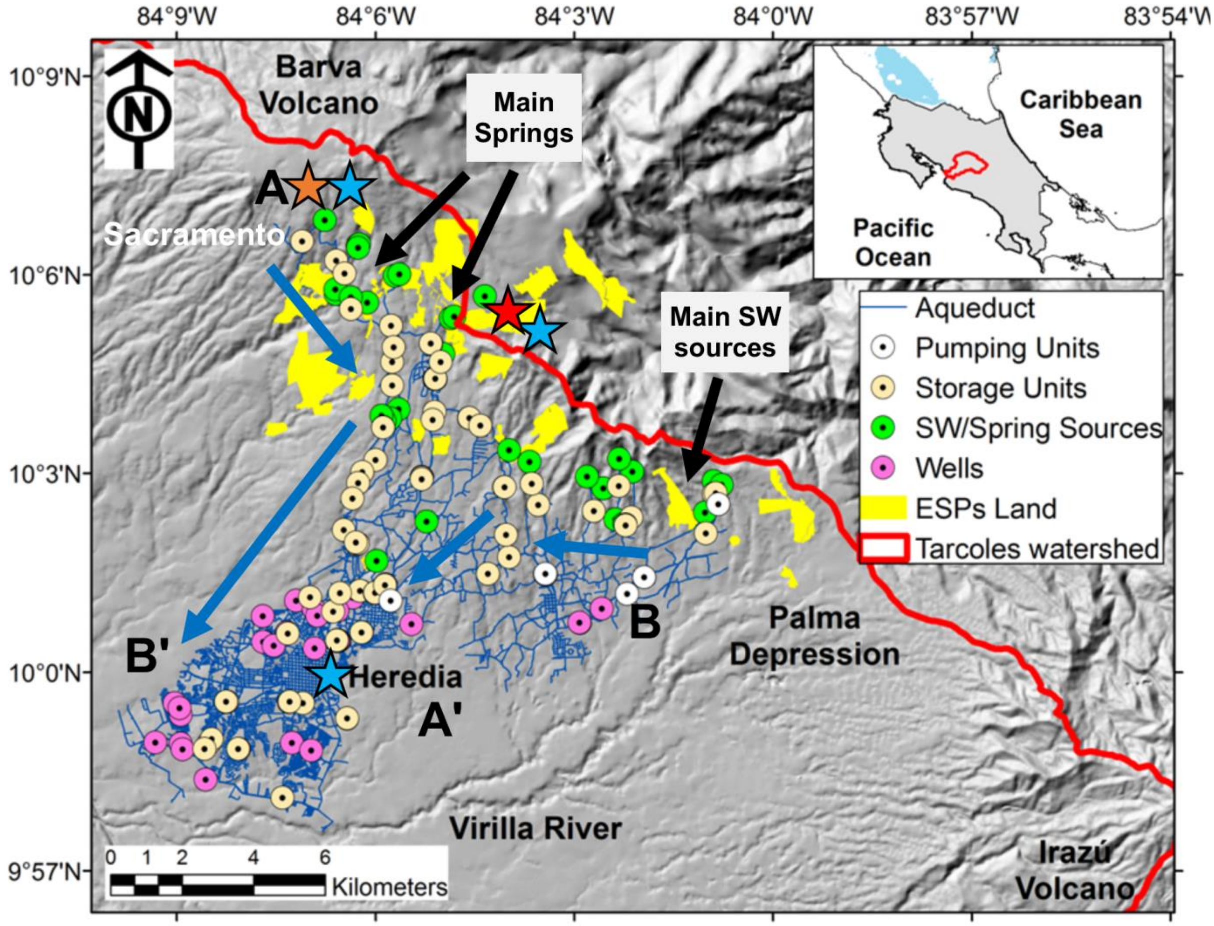

Figure 1: Water distribution system including spring/surface water sources (green), wells (pink), transfer lines (white), and storage units/tanks (light orange). The red bold line denotes the limits of the Virilla/Tárcoles watershed within the continental divide (Pacific versus Caribbean slopes). Yellow polygons represent private properties under the Environmental Services Payment scheme [23] within the most important recharge area. Blue lines represent the pipeline network with an estimated length of 945 km. Heredia is the main city within the aqueduct structure. Blue stars denote rainfall collection sites in the urban area (Heredia) and headwaters (west and east sites). Orange and red stars denote spring and surface monitoring sites. Inset shows the relative location of the study area in central Costa Rica. Lithological cross sections between A-A' and B-B' are presented in the upper panel of Fig. 2. Blue bold arrows indicate main water paths from headwater sources to the lowland urban area. The area is located between two volcano edifices (Barva and Irazú) separated by a wind pass (NE prevailing winds) known as Palma Depression.

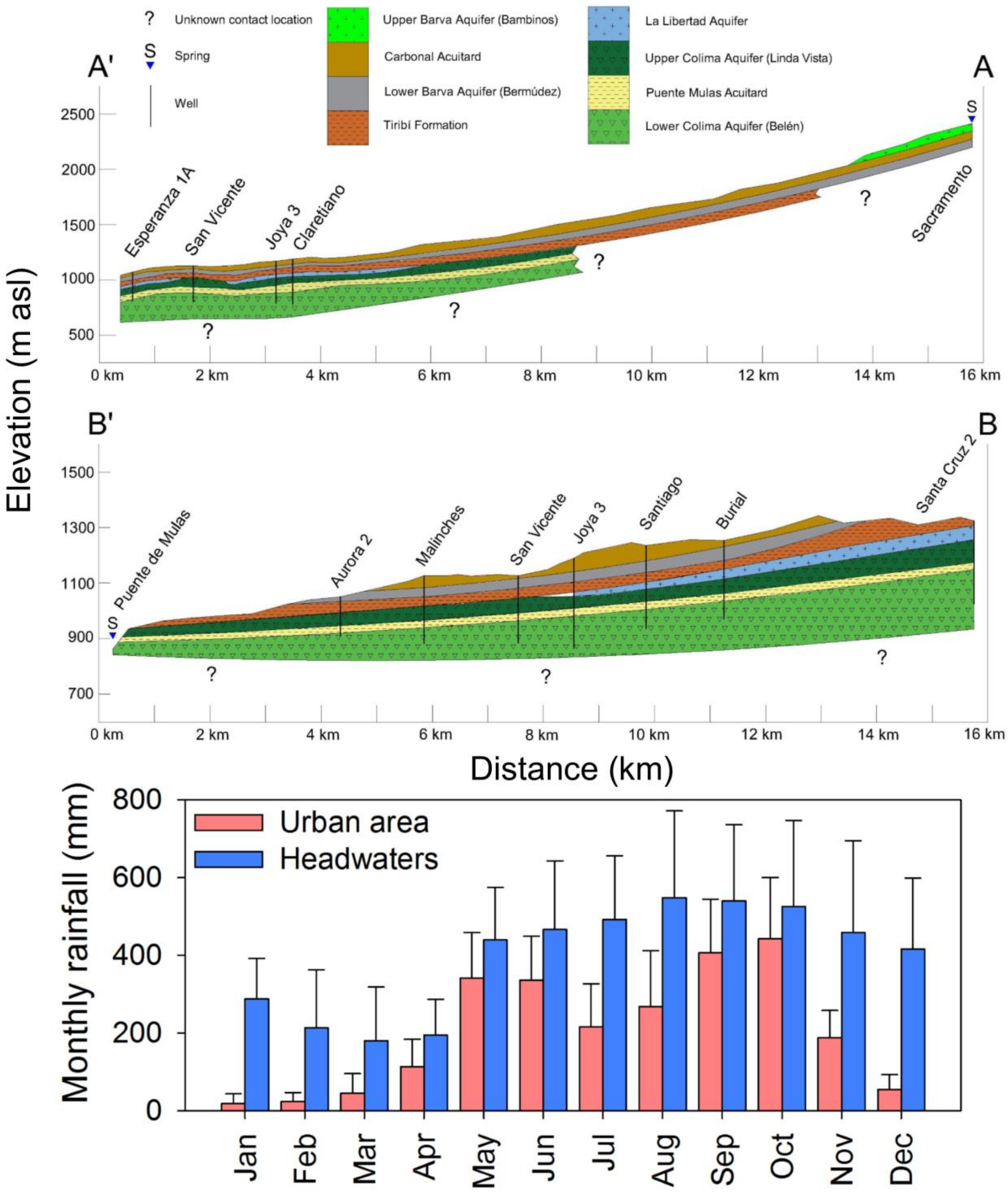

Figure 2: Upper panel) Lithological cross sections of transects A-A' (N-S) and B-B' (E-W) within the study area (See Fig. 1). This multi-aquifer system comprises one unconfined aquifer (Barva) and two deeper semi-confined aquifers (Colima) [24]. Lower panel) Long-term monthly rainfall (mm) within the headwaters of Barva volcano (blue bars) and the urban area of Heredia (pink bars). Error bars denote (1σ) long-term monthly standard deviations.

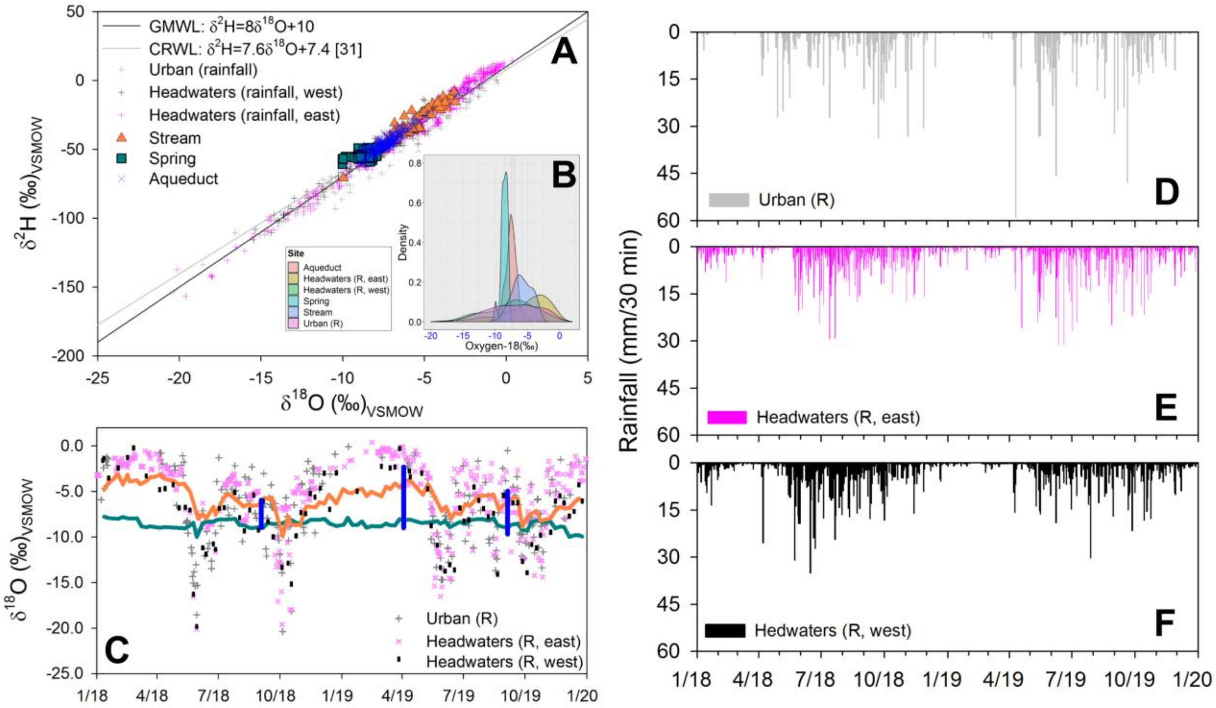

Figure 3: A) Dual isotope diagram including rainfall (R; three sites, color and symbol-coded), stream (orange triangle), spring (dark green square), and aqueduct (blue thin cross) (See location in Fig. 1). The Global Meteoric Water Line (GMWL) [32] and Costa Rican Meteoric Water Line (CRMWL) [31] are included as references. B) Inset shows a density distribution plot for all sources. Dash lines denote median values per source. C) Temporal isotope variations per source. Color coded bold lines represent stream (orange), spring (dark green), and aqueduct (vertical blue lines) time series. Isotope variability in rainfall is symbol coded. D-F) Rainfall (mm/30 min) at the urban and headwater locations.

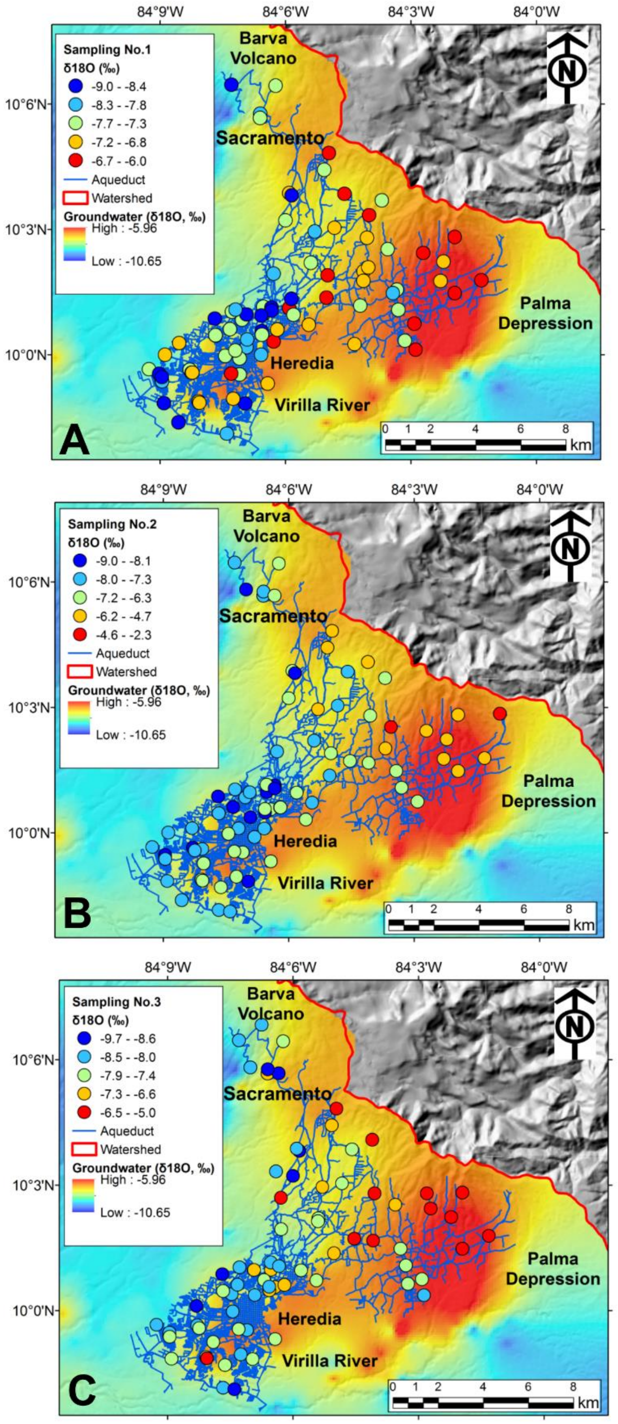

Figure 4: Distribution of $\delta^{18}O$ (‰) across the aqueduct during A) September 2018 (wet season); B) April 2019 (dry season), and C) September 2019 (wet season). A background groundwater isoscape [19] and pipeline network are presented as references.

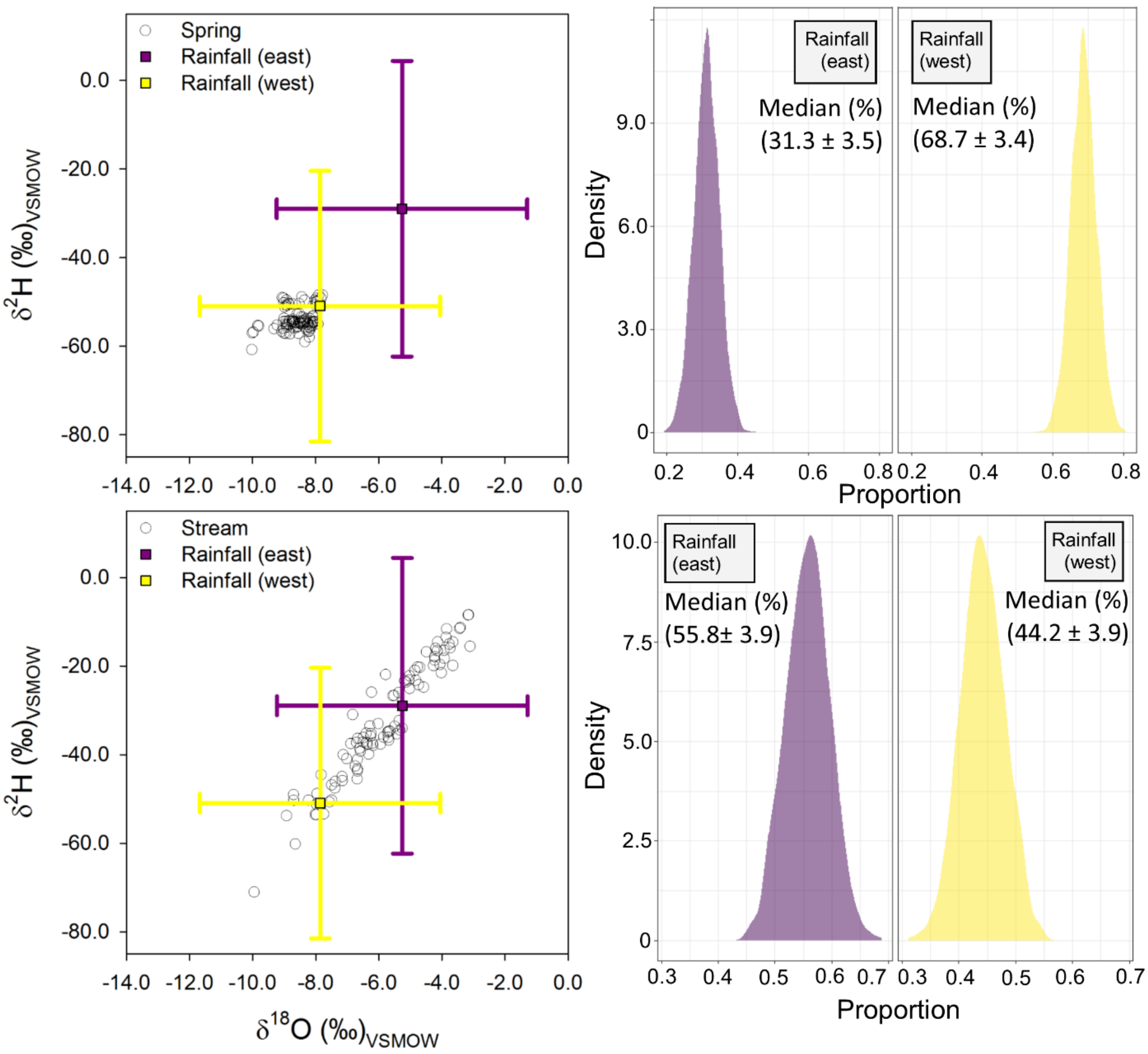

Figure 5: Left panel shows dual isotope diagrams for both mixtures (spring and stream; black empty circles) and mean values of two endmembers (rainfall east and west; purple and yellow squares and error bars, respectively). Right panel shows density plots relative to the proportion of each endmember.

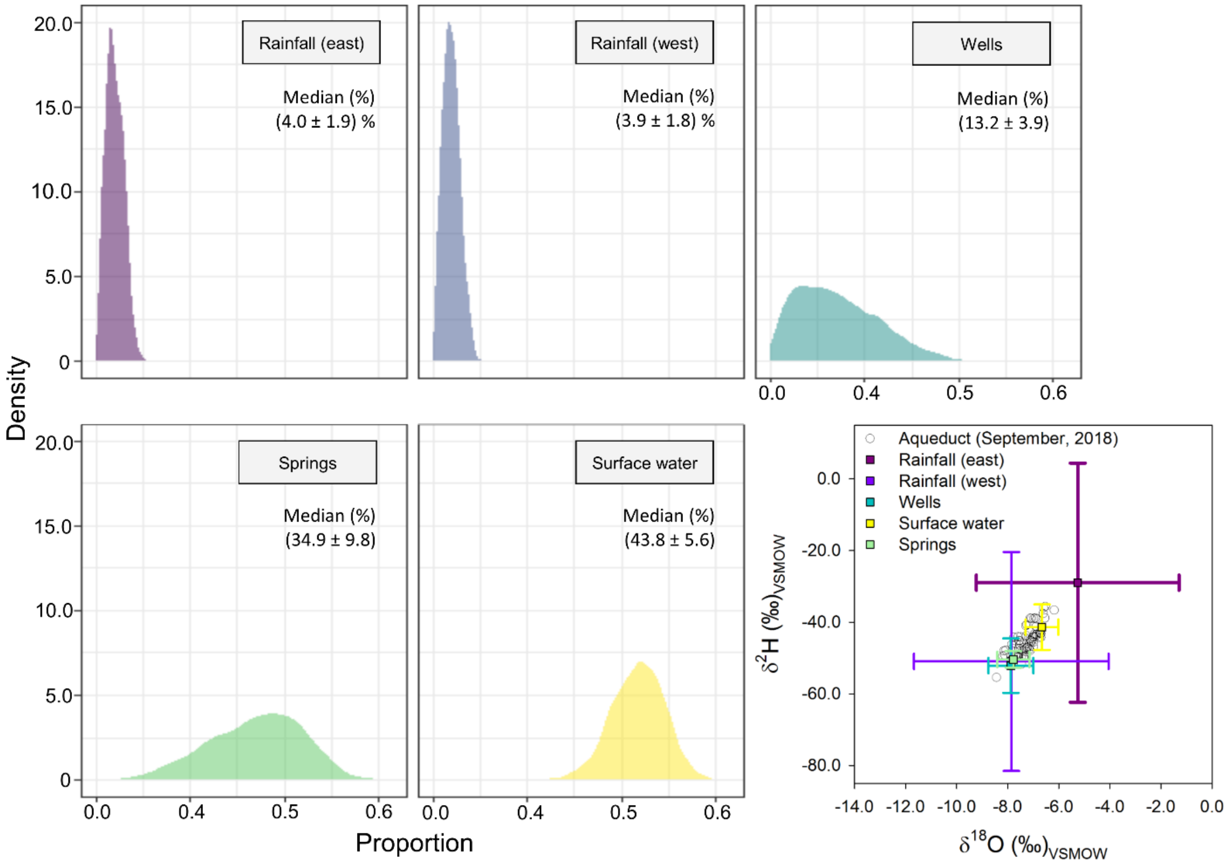

Figure 6: Density plots relative to the proportion of each endmember across the aqueduct during September 2018 and dual isotope diagram for aqueduct mixture (black empty circles) and mean values of five endmembers. Median contributions of each endmember and uncertainties are also reported.

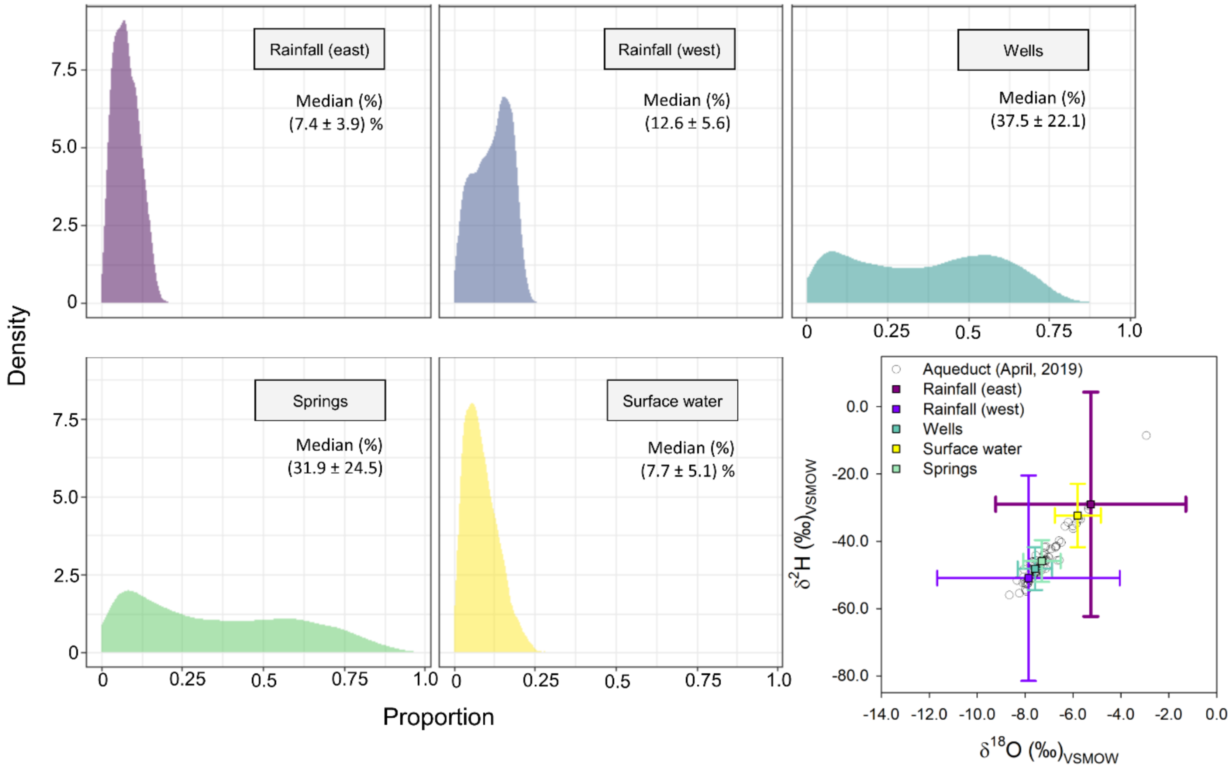

Figure 7: Density plots relative to the proportion of each endmember across the aqueduct during April 2019 and dual isotope diagram for aqueduct mixture (black empty circles) and mean values of five endmembers. Median contributions of each endmember and uncertainties are also reported.

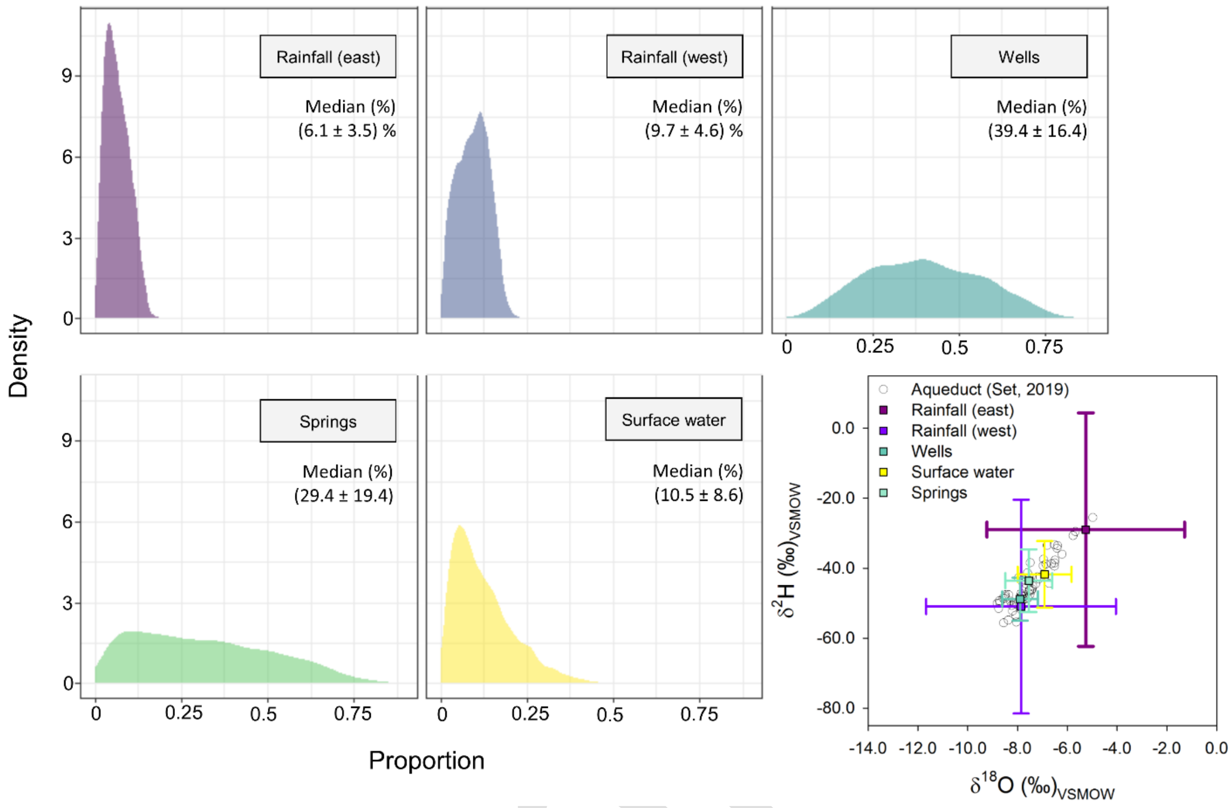

Figure 8: Density plots relative to the proportion of each endmember across the aqueduct during September 2019 and dual isotope diagram for aqueduct mixture (black empty circles) and mean values of five endmembers. Median contributions of each endmember and uncertainties are also reported.

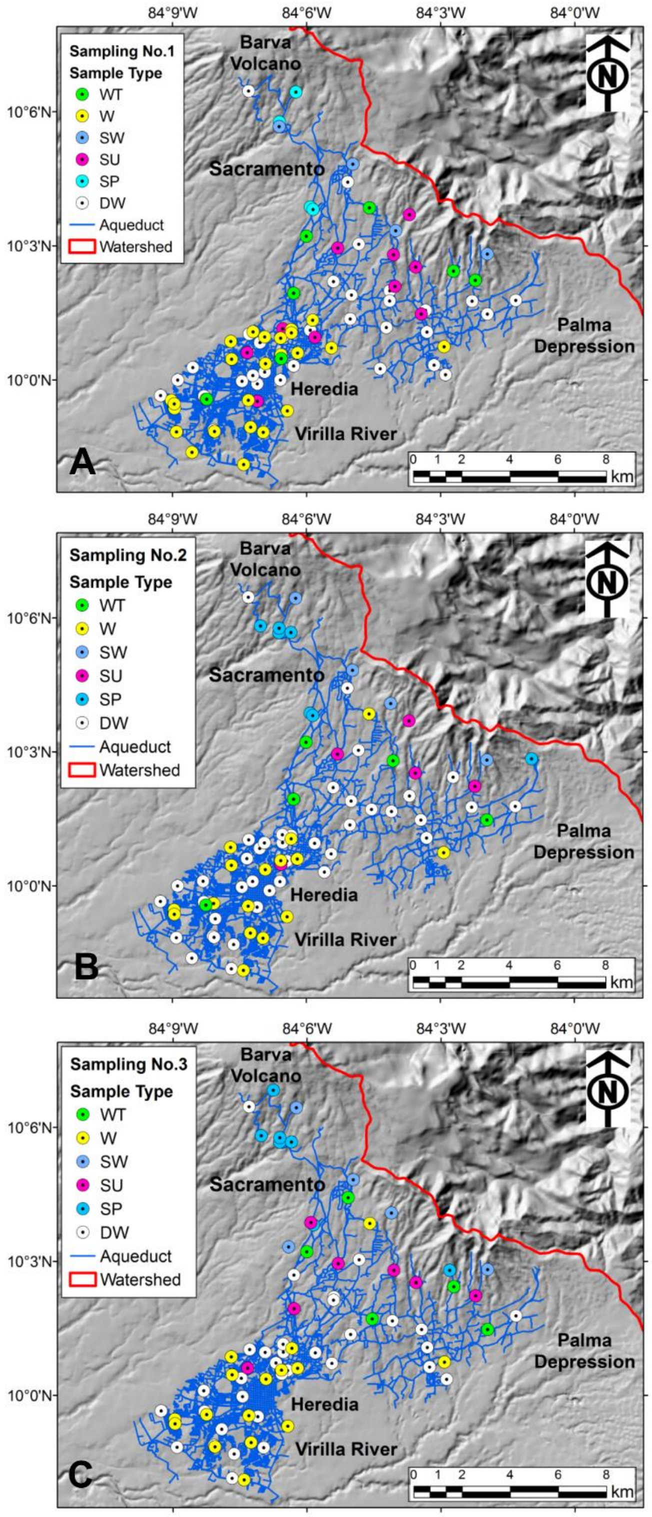

Supplementary Figure 2: Sampling locations by different water source and aqueduct feature. Panels A, B, and C correspond to September (2018), April (2019), and September (2019).

Table S1: Descriptive isotope statistics for each endmember.

Endmember	**$\delta^{18}O$ (‰) (±1σ)**	**$\delta^{2}H$ (‰) (±1σ)**
Rainfall (west)	-7.86±3.81	-51.0±30.6
Rainfall (east)	-5.26±3.97	-29.0±33.4
Sampling 1 (wet season 2018)		
Springs	-7.68±0.63	-50.4±2.3
Wells	-7.88±0.88	-52.1±7.6
Surface waters	-6.66±0.64	-41.4±6.4
Sampling 2 (dry season 2019)		
Springs	-7.30±0.78	-45.9±6.2
Wells	-7.59±0.72	-48.1±6.4
Surface waters	-5.80±0.96	-32.3±9.4
Sampling 3 (wet season 2019)		
Springs	-7.55±0.94	-43.6±1.0
Wells	-7.90±0.72	-48.9±6.1
Surface waters	-6.91±1.08	-41.8±9.5